

Chip-to-chip optical interconnects based on flexible integrated photonics

Lan Li^a, Yi Zou^a, Hongtao Lin^a, Juejun Hu^{*a}, Xiaochen Sun^b, Ning-Ning Feng^b, Sylvain Danto^c, Kathleen Richardson^c, Tian Gu^d, Michael Haney^d

^aDepartment of Materials Science and Engineering, University of Delaware, Newark, DE USA 19716; ^bLaXense Inc., R&D, Walnut, CA USA 91789; ^cCollege of Optics & Photonics, University of Central Florida, Orlando, FL USA 32816-2700; ^dDepartment of Electrical Engineering, University of Delaware, Newark, DE USA 19716

ABSTRACT

A high bandwidth density chip-to-chip optical interconnect architecture is analyzed. The interconnect design leverages our recently developed flexible substrate integration technology to circumvent the optical alignment requirement during packaging. Initial experimental results on fabrication and characterization of the flexible photonic platform are also presented.

Keywords: Optical interconnects, energy efficiency, flexible photonics, nanoimprint, waveguides, resonators, adhesive bonding

1. INTRODUCTION

Progress in high-performance computing (HPC) is driving an increasing demand for high speed and energy efficient data communication solutions. Traditional copper wiring technology is quickly approaching its fundamental limit set forth by resistive power dissipation, RC delay, and cross talk. Optical interconnects, which already dominate long-haul telecommunications, have emerged as a promising solution to the "interconnect bottleneck" and are being implemented at ever decreasing distances. Over the past decade, routers in data centers and HPC systems have adopted fiber optics to meet the rack-to-rack I/O performance requirements. Nowadays, board-level interconnects based on parallel optics, where data are simultaneously transmitted along more than one optical lane, have become a preferred interconnect solution over copper cables for HPC given their reduced power consumption, low weight, and large bandwidth capacity. A number of optical interconnect architectures have been investigated including multi-core fiber interconnects [1], optical printed circuit boards [2, 3], silicon photonics [4, 5], and hybrid approaches [6-11]. In this paper, we propose and analyze a new chip-to-chip interconnect scheme based on a flexible photonics platform we recently developed. Our design offers scalable high bandwidth density and potentially enables a simplified packaging solution without involving optical alignment. Single mode high-index contrast waveguides were fabricated through a thermal nanoimprint patterning process in chalcogenide glass (ChG) films. The low deposition and glass transition temperatures of ChGs make our optical waveguide fabrication process fully compatible with flexible substrate integration. Mechanical flexibility against mechanical deformation was also evaluated by monitoring the optical performance of waveguide-coupled microdisk resonators in-situ during bending. Finally, we developed polymer planarization and adhesive bonding processes to enable the full integration of flexible chip-to-chip interconnects.

2. INTERCONNECT SYSTEM LAYOUT

Figure 1 schematically illustrates the interconnect design. The interconnect architecture builds on a flexible planar photonic link, which consists of an array of single-mode glass optical waveguides on a common flexible substrate as well as active optoelectronic components (lasers and detectors) bonded onto the flexible substrate and optically coupled to the waveguides. The active devices based on an alignment-free die-to-wafer bonding process [12-14] and are directly coupled to the waveguides. Two ends of the flexible link is flip-chip bonded and electrically connected to chips through solder bumps and on-chip metal vias, which also serve as effective heat conduction channels between the active devices

*hujuejun@udel.edu; phone 1 302 831-6878; fax 1 302 831-4545.

and the chip. The flexible link interconnects present several unique advantages for chip packaging, such as simplified packaging, large bandwidth density, and low power consumption [15], which we will elaborate in the following sections.

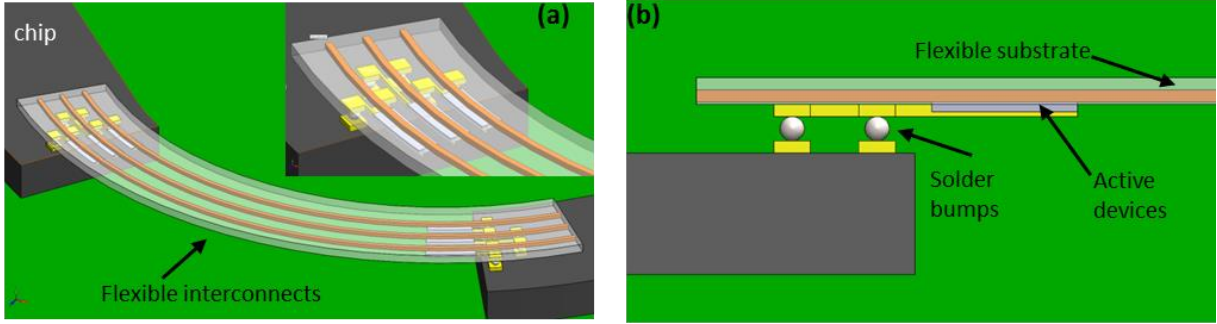


Figure 1. The fully-integrated flexible optical interconnect design: (a) schematic tilted view of a flexible optical link bonded to a chip; (b) cross-sectional structure of the optical link.

2.1 Simplified packaging

Stringent alignment accuracy is often cited as the main argument against the use of single-mode waveguides; however, our interconnect link is embedded in polymer substrate, providing enough flexibility for the misalignment between chips surface-mounted on carriers or on a printed circuit board. Besides, no optical alignment is required since the optical link only interfaces with the chips electronically. Figure 1b shows the cross section structure of the optical link. Specifically, the active devices are directly coupled to the waveguides based on an alignment-free die-to-wafer bonding process. And the active dies can be thinned down to a small thickness ($< 25 \mu\text{m}$) to achieve both the evanescently coupling and low-profile bonding, providing an enough height space for the electronic connection of flexible interconnects through a flip-chip bonding process [15].

2.2 Large bandwidth density

Table 1. Bandwidth scalability of our flexible optical interconnect platform as compared to other competing optical interconnect technologies

Technology	Waveguide pitch (μm)	Total I/O channel #	Aggregate data rate (Tb/s)
Flexible optical interconnect	10	5,000	100
Polymer optical fiber ribbons [16]	250	200	4
Multi-mode on-board waveguides [17, 18]	62.5	800	16
Multi-mode off-board waveguides [19, 20]	200	250	5

As shown in Figure 1, the interconnect bandwidth density will only be limited by the physical size of on-chip contact pads and solder bumps. Specifically, the bandwidth density can be dramatically increased by arranging the on-chip contact pads in 2-D arrays. In addition, the use of high-index-contrast single-mode waveguides for optical interconnects also contributes to high-density integration. To more clearly present our approach's bandwidth scalability benefit, we compare the possibly attainable aggregate bandwidths of several interconnect solutions in Table 1. We assume: 1) a bonding pad pitch of $100 \mu\text{m}$ which is readily achievable using flip chip bonding [21]; 2) 10 Gb/s single channel data rate; 3) $2.5 \text{ cm} \times 2.5 \text{ cm}$ chip size; 4) all four chip edges are used for interconnects. It is apparent that the bandwidth density of traditional 1-D edge-coupling optical interconnect schemes are limited by the physical size of the chip to < 20

Tb/s, while our approach enables off-chip I/O bandwidth scalable to 100 Tb/s which sufficiently accommodates the interconnect bandwidth need at 9 nm CMOS node [15].

2.3 Low power consumption

Table 2. Optical loss budget (in dB) of the flexible interconnect platform (projected) and typical VCSEL-based multi-mode optical links

Loss mechanisms	Flexible single-mode photonics	VCSEL-based multi-mode optics
Laser-to-waveguide coupling loss	0	1.1 [22]
Modulator insertion loss	1 [23]	0
Waveguide-to-PD coupling loss	0.5 [24]	1.1 [22]
Waveguide propagation loss	4 [25]	0
Extinction ratio penalty	3	3
Margin	4	4
Total	12.5	9.2

In addition to these packaging benefits and large bandwidth density, the flexible interconnect platform also offers low power consumption comparable or even superior to that of high-performance VCSEL-based links. Table 2 compares the estimated optical loss budget of our technology with that of VCSEL-based multi-mode optics which includes the three current technology platforms listed in Table 1. The numbers listed in the table are based on values previously reported in literature. Since the evanescent lasers used in the flexible photonic links are waveguide coupled, the laser-waveguide coupling loss vanishes as it becomes part of the laser efficiency. These numbers indicate comparable optical loss for both types of interconnect links and support a low power laser source owing to high sensitivity of modern receivers (typically better than -18 dBm at 10 Gb/s [26]). In our case, the required output optical power of a continuous-wave (CW) bonded laser is -5.5 dBm so laser power consumption is currently dominated by relatively large threshold power (~30 mW [27]) due to less mature fabrication processes. Certainly the hybrid laser integration technology is still much less developed to date compared to VCSELs and significant improvements are thus expected by design and processing optimization. On the other hand, most VCSELs are directly modulated because of its surface emitting configuration. A VCSEL has to be pumped to high output power in order to be modulated at a high data rate of 10 Gb/s. Direct modulation of a state-of-the-art VCSEL at 10 Gb/s typically requires ~15 mW [28] laser power. Figure 2 compares the single channel power consumption at 10 Gb/s for our technology and that of VCSEL-based links. Since our approach employs external modulators, using a single bonded laser for different channels will further reduce the power consumption, which largely mitigates the high threshold power issue plaguing bonded lasers. In addition, when considering the electrical circuits driving the optical devices, our approach has significant advantage in power consumption because the electroabsorption modulators (equivalent to reverse-biased diodes) used in this case requires much lower power driver circuits compared to VCSEL's driver circuits which switch at very high current levels. The overall link power consumption is thus expected to be lower in our approach than in the VCSEL approach [15].

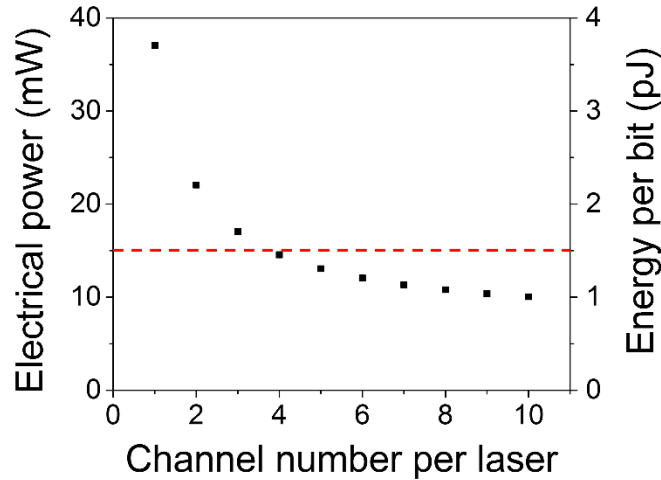


Figure 2. Single channel electrical power consumption of the flexible optical link: the horizontal axis denotes the number of channels sharing a single bonded laser. The dotted line indicates the single-channel electrical power consumption of VCSEL-based multi-mode optical links. The assumptions are: 1) 10 Gb/s single-channel data rate; 2) each channel is individually encoded using a modulator with 100 fJ/bit power consumption; 3) receiver sensitivity is -18 dBm; and 4) the bonded laser has a threshold power of 30 mW and 4% slope efficiency [27].

3. EXPERIMENT RESULTS AND DISCUSSIONS

3.1 Flexible photonic interconnect platform fabrication and photonics devices characterization

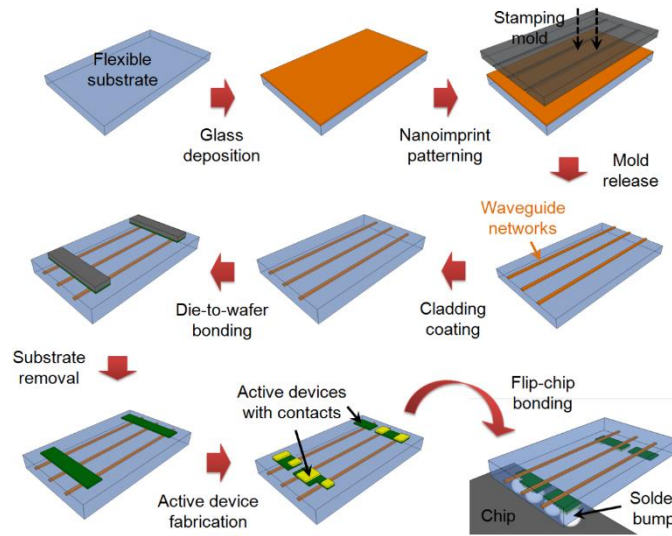


Figure 3. Fabrication process of the flexible photonics interconnect platform

We choose to use chalcogenide glasses (ChGs, amorphous compounds containing S, Se or Te) as the waveguide material given their high and tunable (by adjusting their compositions) refractive indices, superior transparency at the 1550 nm telecommunication wavelength and low deposition transition temperature.

Figure 3 illustrates the proposed fabrication process flow of the flexible photonic link platform. The glass films are deposited using thermal evaporation, followed by thermal nanoimprint using an elastomer stamp to pattern the waveguide link networks on polyimide (PI) plastic substrates. During deposition, the substrate was kept near room temperature ($< 50\text{ }^{\circ}\text{C}$). More details concerning the bulk glass preparation [29] and film deposition processes may be

found elsewhere [30, 31]. The elastomer stamps for imprint are fabricated following standard replica molding protocols. To minimize optical scattering loss caused by sidewall roughness, lithographically defined resist patterns used for replica molding underwent a thermal reflow step to remove residual surface roughness via the interaction of surface tension. Waveguides produced using the process feature a smooth surface finish with sub-nm RMS roughness and low optical loss. The imprint was then performed in a N₂ purged glove box by pressing PDMS stamps against glass thin film samples under a constant pressure of 0.13 MPa and a temperature of 250 °C for 25 min. Figure 4a shows a fabricated flexible photonic waveguide sample. Lastly, an SU-8 polymer (MicroChem Inc.) layer was spin coated on the imprinted structures to protect the devices against surface oxidation and also serve as an adhesive bonding agent for subsequent III-V die attachment. The active devices are fabricated using alignment-free "die-to-wafer" bonding, a process that has been successfully employed to demonstrated III-V heterogeneous integration on Si [12, 14]. In the last step, the flexible link is flip-chip bonded onto chips to complete the fabrication process [15].

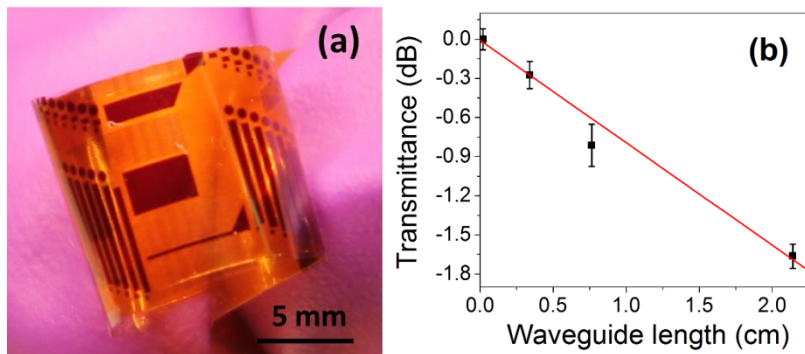


Figure 4. (a) Photo of a flexible waveguide sample; (b) dots: measured transmitted intensity as a function of device length; slope of the fitted line yields a waveguide loss of (0.8 ± 0.3) dB/cm.

Optical transmission characteristics of the waveguides at 1550 nm wavelength were measured using an Agilent/HP 81680A external cavity tunable laser. Paper-clip patterns with different waveguide lengths were used for loss evaluation. Figure 4b shows the transmitted intensity (averaged over 9 different waveguides) as a function of waveguide lengths. Propagation loss can be inferred from the slope of the curve to be (0.8 ± 0.3) dB/cm. Surface morphology of the imprinted waveguides was characterized using atomic force microscopy prior to SU-8 coating, which yielded an average surface RMS roughness of 0.7 nm [15]. The smooth surface finish inherited from the reflow treated resist pattern contributes to the low optical loss measured in our devices: simple scattering loss estimation using the Payne-Lacey theory [32] indicates that roughness scattering accounts for < 0.1 dB/cm in the waveguide loss, and therefore the majority of the loss contribution comes from material attenuation and discrete defects on the substrates, both of which are expected to be mitigated through further processing optimization.

The mechanical flexibility of the fabricated photonic devices was also quantified. According to our nano-mechanical analysis [33], PI-silicone-PI tri-layer films was used as the flexible substrate since the the low Young's modulus (~ 2 MPa) silicone rubber layer serves as an effective agent to relieve strain on the PI layer surfaces where the photonic devices reside during bending deformation, thus enabling superior mechanical robustness of the flexible photonic waveguide devices. To test the mechanical reliability of our flexible photonic devices, we fabricated a series of pulley-coupled micro-disk resonators [34] on flexible substrates and tested their optical performance when the devices underwent mechanical deformation. Figure 5 plots the resonator Q-factors and extinction ratios as functions of bending curvature, measured when the devices were bent. The test revealed no measurable optical performance degradation within our measurement error. We further tested the devices' optical performance after multiple bending cycles at 0.5 mm bending radius, and little change was observed even after 100 bending cycles [33]. Optical microscope observation further revealed the absence of micro-cracks or delamination in the layers, which clearly indicate that our devices are robust against mechanical deformation.

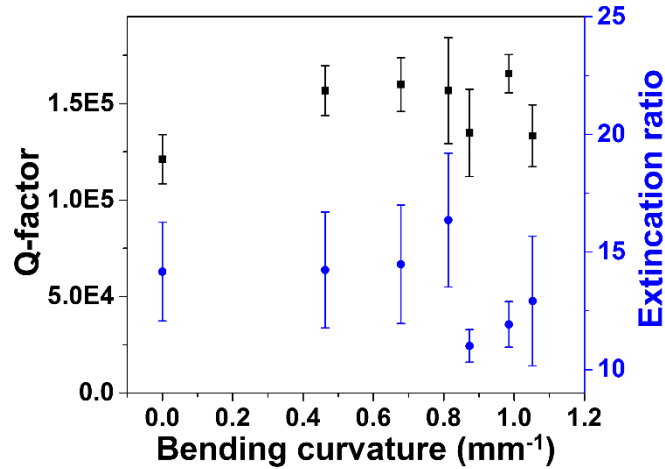


Figure 5. Loaded Q-factors and extinction ratios of flexible micro-disk glass resonators as functions of bending curvature measured during bending.

3.2 III-V die bonding on flexible substrates

We adopted an adhesive die bonding process for active component integration on flexible substrates. Since the bonding process use unpatterned III-V semiconductor die rather than fabricated III-V active devices, no alignment is required in the bonding step. The III-V die with multiple quantum well (MQW) active layers are patterned to form active components only after bonding, and alignment of the III-V devices to the glass waveguides underneath is guaranteed in the lithographic patterning process.

As for the integration of passive waveguides to the active devices, we used SU-8 photoresist as the adhesive agent to facilitate the bonding process. Therefore, planarization of SU-8 on waveguides and bonding quality are both important for the integration process. Through optimized heat treatment to control the SU-8 cross-link process, we developed an ultra-thin (30 nm overcoating) epoxy planarization process on top of a $\text{Ge}_{23}\text{Sb}_7\text{S}_{70}$ glass waveguide (Figure 6a). Degree of planarization (DOP) measured from the SEM image is 98%, an amazingly high number considering the small planarization coating thickness.

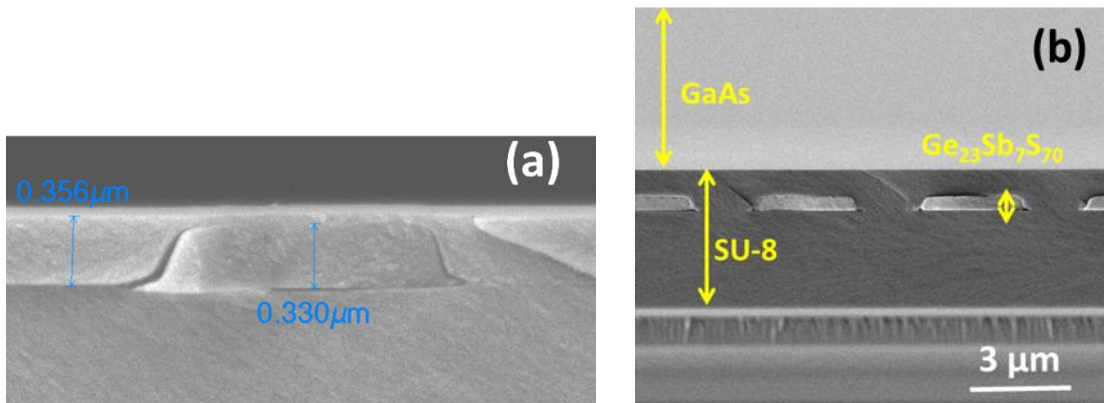


Figure 6. (a) SEM cross-sectional image of a Ge-Sb-S glass waveguide with a planarizing SU-8 overcoating showing a high DOP of 98%; (b) SEM cross-sectional image of the bonded GaAs dice after substrate thinning, showing excellent interface adhesion free of delamination.

In addition to the excellent planarization capability of SU-8 on waveguides, SU-8 layer also functions as an adhesive agent for III-V active device bonding. The thermal treatment during bonding triggered thermal cross-linking of SU-8 to transform the layer into a mechanically robust adhesive between the III-V die and the flexible substrate. The III-V substrate was subsequently removed by mechanical thinning to $\sim 15 \mu\text{m}$ thickness followed by chemical etching to

create a semiconductor nanomembrane containing the MQW active region. It has been well established that semiconductor nanomembranes can be highly flexible despite the intrinsic rigidity of its constituent semiconductor material, making it compatible with flexible substrate integration. Figure 7 shows photos of a bonded, unpatterned GaAs dice before and after mechanical thinning on a polisher equipped with a custom-designed precision thickness control accessory. As shown in Figure 6b, no delamination was observed at the bonding interface after the mechanical thinning process. Future work will involve chemical thinning of the III-V substrate following mechanical lapping to create thin active MQW structures optically coupled to waveguides for a full photonic link demonstration.

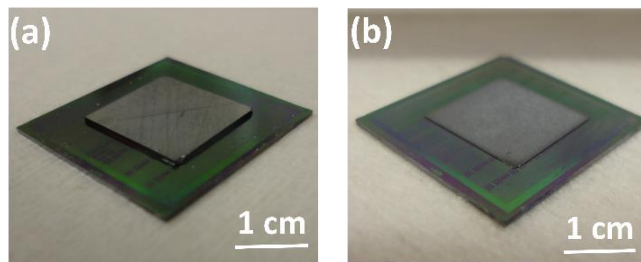


Figure 7. Photos of a bonded GaAs dice on Ge-Sb-S waveguides before (a) and after (b) substrate thinning.

4. CONCLUSIONS

Compared to current chip-to-chip optical interconnect architectures using fibers or multi-mode waveguides, our optical interconnect design have the following advantages: 1) simplified packaging process; 2) large bandwidth density; 3) low power consumption; and 4) superior mechanical flexibility. We have also experimentally validated an adhesive bonding process for III-V active photonic integration on flexible substrates. Our future efforts will focus on the demonstration of a novel planar, flexible optical interconnect platform with fully-integrated optoelectronic functionalities.

REFERENCES

- [1] Li, M.-J., Hoover, B., Nazarov, V. N. *et al.*, "Multicore fiber for optical interconnect applications," Opto-Electronics and Communications Conference (OECC), 2012 17th, 564-565 (2012).
- [2] Van Steenberge, G., Geerinck, P., Van Put, S. *et al.*, "MT-compatible laser-ablated interconnections for optical printed circuit boards," Journal of Lightwave Technology 22(9), 2083-2090 (2004).
- [3] Bona, G. L., Offrein, B. J., Bapst, U. *et al.*, "Characterization of parallel optical-interconnect waveguides integrated on a printed circuit board," Proc. SPIE 5453, 135 (2004).
- [4] Krishnamoorthy, A. V., Ho, R., Zheng, X. *et al.*, "Computer systems based on silicon photonic interconnects," Proceedings of the Ieee 97(7), 1337-1361 (2009).
- [5] Batten, C., Joshi, A., Orcutt, J. *et al.*, "Building many-core processor-to-DRAM networks with monolithic CMOS silicon photonics," IEEE Micro 29(4), 8-21 (2009).
- [6] Chen, R. T., Lin, L., Choi, C. *et al.*, "Fully embedded board-level guided-wave optoelectronic interconnects," Proceedings of the Ieee 88(6), 780-793 (2000).
- [7] Liu, Y., Lin, L., Choi, C. *et al.*, "Optoelectronic integration of polymer waveguide array and metal-semiconductor-metal photodetector through micromirror couplers," Photonics Technology Letters, IEEE, 13(4), 355-357 (2001).
- [8] Haney, M., Nair, R., and Gu, T., "Chip-scale integrated optical interconnects: a key enabler for future high-performance computing," SPIE OPTO, 82670X-82670X-12 (2012).
- [9] Nair, R., Gu, T., and Haney, M. W., "Hybrid chip-scale optical interconnects using multiple quantum well devices bonded to silicon," Optical Interconnects Conference, 2012 IEEE 18-19 (2012).
- [10] Gu, T., Nair, R., and Haney, M. W., "Chip-level Multiple Quantum Well Modulator-based Optical Interconnects," Journal of Lightwave Technology 31(24), 4166-4174 (2013).
- [11] Gu, T., Nair, R., and Haney, M. W., "Prismatic coupling structure for intrachip global communication," IEEE Journal of Quantum Electronics 45(4), 388-395 (2009).
- [12] Liang, D., Roelkens, G., Baets, R. *et al.*, "Hybrid integrated platforms for silicon photonics," Materials 3(3), 1782-1802 (2010).

- [13] Roelkens, G., Brouckaert, J., Van Thourhout, D. *et al.*, "Adhesive Bonding of InP / InGaAsP Dies to Processed Silicon-On-Insulator Wafers using DVS-bis-Benzocyclobutene," *Journal of the Electrochemical Society* 153(12), G1015-G1019 (2006).
- [14] Roelkens, G., Van Campenhout, J., Brouckaert, J. *et al.*, "III-V/Si photonics by die-to-wafer bonding," *Materials Today* 10(7), 36-43 (2007).
- [15] Li, L., Zou, Y., Lin, H. T. *et al.*, "A Fully-Integrated Flexible Photonic Platform for Chip-to-Chip Optical Interconnects," *Journal of Lightwave Technology* 31(24), 4080-4086 (2013).
- [16] BOCKSTAELE, M. D. W., "Chip-to-chip parallel optical interconnects over optical backpanels based on arrays of multimode waveguides," *Proceedings of the 9th Annual Symposium of the IEEE/LEOS Benelux Chapter*, 61-64 (2004).
- [17] Doany, F. E., Schow, C. L., Kash, J. A. *et al.*, "Waveguide-coupled parallel optical transceiver technology for Tb/s-class chip-to-chip data transmission," *Integrated Optoelectronic Devices*, 68990V-68990V-7 (2008).
- [18] Schares, L., Kash, J. A., Doany, F. E. *et al.*, "Terabus: Terabit/second-class card-level optical interconnect technologies," *IEEE Journal of Selected Topics in Quantum Electronics*, 12(5), 1032-1044 (2006).
- [19] Bosman, E., Van Steenberge, G., Hendrickx, N. *et al.*, "Flexible embedded active optical link," *Photonics Europe*, 69920V-69920V-10 (2008).
- [20] Shibata, T., and Takahashi, A., "Flexible opto-electronic circuit board for in-device interconnection," *Electronic Components and Technology Conference*, 2008. ECTC 2008. 58th, 261-267 (2008).
- [21] Gan, H., Wright, S., Polastre, R. *et al.*, "Pb-free microjoints (50/spl mu/m pitch) for the next generation microsystems: the fabrication, assembly and characterization," *Electronic Components and Technology Conference*, 2006. *Proceedings*. 56th, 6 pp (2006).
- [22] Young, I. A., Mohammed, E., Liao, J. T. S. *et al.*, "Optical I/O Technology for Tera-Scale Computing," *IEEE Journal of Solid-State Circuits* 45(1), 235-248 (2010).
- [23] Hofrichter, J., Raz, O., La Porta, A. *et al.*, "A low-power high-speed InP microdisk modulator heterogeneously integrated on a SOI waveguide," *Opt. Express* 20(9), 9363-9370 (2012).
- [24] Ahn, D., Hong, C.-y., Liu, J. *et al.*, "High performance, waveguide integrated Ge photodetectors," *Opt. Express* 15(7), 3916-3921 (2007).
- [25] Madden, S. J., Choi, D. Y., Bulla, D. A. *et al.*, "Long, low loss etched As₂S₃ chalcogenide waveguides for all-optical signal regeneration," *Opt. Express* 15(22), 14414-14421 (2007).
- [26] WTD, "10Gb/s PIN-TIA ROSA PTCM992-405," (2009). <http://www.wtd.com.cn/en/uploadfile/ptcm992-405.pdf>
- [27] Lamponi, M., Keyvaninia, S., Jany, C. *et al.*, "Low-threshold heterogeneously integrated InP/SOI lasers with a double adiabatic taper coupler," *Photonics Technology Letters, IEEE*, 24(1), 76-78 (2012).
- [28] JDSU, "JDSU 850 nm 10 G connectorized transmit optical sub-assembly (TOSA)," (2012). <http://www.jdsu.com/ProductLiterature/pl-xxd-00-s40-cx-ds-oc-ae.pdf>
- [29] Petit, L., Carlie, N., Adamietz, F. *et al.*, "Correlation between physical, optical and structural properties of sulfide glasses in the system Ge-Sb-S," *Materials Chemistry and Physics* 97(1), 64-70 (2006).
- [30] Hu, J. J., Tarasov, V., Agarwal, A. *et al.*, "Fabrication and testing of planar chalcogenide waveguide integrated microfluidic sensor," *Optics Express* 15(5), 2307-2314 (2007).
- [31] Lin, H., Li, L., Zou, Y. *et al.*, "Demonstration of high-Q mid-infrared chalcogenide glass-on-silicon resonators," *Opt. Letters* 38(9), 1470-1472 (2013).
- [32] Lacey, J., and Payne, F., "Radiation loss from planar waveguides with random wall imperfections," *IEEE Proceedings J of Optoelectronics* 137, 282-288 (1990).
- [33] Li, L., Lin, H., Qiao, S. *et al.*, "3-D Integrated Flexible Glass Photonics," arXiv:1307.5937v2 (2013). <http://arxiv.org/abs/1307.5937v2>
- [34] Hu, J., Carlie, N., Feng, N.-N. *et al.*, "Planar waveguide-coupled, high-index-contrast, high-Q resonators in chalcogenide glass for sensing," *Optics Letters* 33(21), 2500-2502 (2008).